Magnetism dynamics driven by phase separation in Pr-doped manganite thin films: A Ferromagnetic resonance study

D. Carranza-Celis[1], E. Skoropata[2], Amlan Biswas[3], M.R. Fitzsimmons[4,5], Ivan K. Schuller[6] and Juan Gabriel Ramirez[1]

[1]*Department of Physics, Universidad de los Andes, Bogotá 111711, Colombia*

[2]*Materials Science and Technology Division, Oak Ridge National Laboratory, Oak Ridge, TN 37831, USA*

[3]*Department of Physics, University of Florida, Gainesville, Florida 32611 USA*

[4]*Neutron Scattering Division, Oak Ridge National Laboratory, Oak Ridge, TN 37831, USA*

[5]*Department of Physics and Astronomy, University of Tennessee, Knoxville, TN 37996, USA*

[6]*Center for Advanced Nanoscience, Department of Physics, University of California–San Diego, La Jolla, CA, USA*

Abstract

We performed ferromagnetic resonance measurements of a $(La_{1-x}Pr_x)_{1-y}Ca_yMnO_{3-\delta}$ with $x = 0.52 \pm 0.05$, $y = 0.23 \pm 0.04$, and $\delta = 0.14 \pm 0.10$ thin single crystalline film which, in combination with micromagnetic simulations, reveal three temperature regions consistent with i) a ferromagnetic-paramagnetic transition in which ferromagnetic domains nucleate and grow, ii) followed by a filamentary fluid-like percolation of magnetic domains exhibiting dynamic processes and finally, iii) the existence of a blocking temperature below which the magnetism is a metastable glassy-like state with strong decoherence of the uniform resonance mode. Our results suggest a strain-liquid to strain-glass spin order transition in which the magnetism and fluid-like dynamics of the separated phases freeze at low temperatures. We show the magnetism dynamics depend strongly on the phase-separated state and morphology of the magnetic domains suggesting a route to control of phase separation and realization of spintronic and magnonic devices.

An important feature of many manganite systems is electronic and magnetic phase separation (PS) which is responsible for colossal magnetoresistance (CMR) [1–3]. PS can occur due to the coexistence and competition of the ferromagnetic metal (FMM) phase and an antiferromagnetic charge-ordered insulator phase (AFM-COI) that yield a complex phase diagram for the manganites [4,5]. PS has been observed using magnetic force microscopy techniques in archetypical (La,Pr,Ca)—alloyed MnO_3 manganite where PS shows two behaviors: (i) fluid phase separation (FPS) at intermediate temperatures and (ii) static phase separation (SPS) at lower temperatures. In the FPS state the FMM and AFM-COI phases show a dynamic fluid-like behavior—i.e., they have a fluid-like nature due to unpinned boundaries between phases induced by chemical disorder. This implies that the morphology of the separated phases and the mobility of its interfaces may be controlled with external perturbations as voltage, magnetic field, or strain [6–8]. On the other hand, in the SPS state the dynamics of the degrees of freedom (spin, local lattice distortion, etc.) slow down yielding glassy behavior [9–12] and a magnetic cluster glass in the SPS [13]. Magnetism of the FPS state, because it is more fluid, should be more easily controlled with magnetic and electric fields and strain (in thin films systems) [5–7,14] than the SPS state. Further, control of the magnetism may allow manipulation of the propagation properties of spin waves, which is desirable in the design of future magnonic devices operated by voltage [15].

Here, we report ferromagnetic resonance (FMR) measurements of a single crystal manganite film $(La_{1-x}Pr_x)_{1-y}Ca_yMnO_{3-\delta}$ (LPCMO) ($x = 0.52\pm0.05$, $y = 0.23\pm0.04$, $\delta = 0.14\pm0.10$). In this study of FMR with temperature, we observe a clear difference in the spin dynamics between the strain-liquid and strain-glass states. Magnetization and resistance measurements corroborate the difference. We do not observe FMR modes in the strain-glass

state, suggesting decoherence of the uniform resonance mode possibly due to magnetic inhomogeneity in a metastable glassy-like state. Comparisons of micromagnetic simulations to the experimental data reveal an evolution of morphology for the different magnetic phases with temperature. Additionally, the morphology evolves differently for warming or cooling, which could be interpreted as a sign of an energy landscape with a complex profile that depends on the phase competition in an AFM-to-FMM or FMM-to-AFM transition.

The LPCMO thin film of thickness 30 nm was grown using pulsed laser deposition on a $NdGaO_3$ (NGO) (110) substrate. See Ref. [16,17] for details regarding the fabrication and for θ-2θ x-ray diffraction pattern of the LPCMO thin film fabricated with the same conditions than the sample of this work. FMR measurements were performed using a 9.4 GHz electron paramagnetic resonance spectrometer. FMR measurements were taken as a function of temperature in 0.5 K steps for warming and cooling between 200 K and 40 K. A microwave power of 1 mW was used while the dc magnetic field was swept between 0 and 9 kOe at a rate of 10 Oe/s for each temperature. We also measured electrical transport under similar temperature and dc fields (between 0 and 9 kOe) sweep rates. Magnetization measurements with magnetization and applied field applied along the surface normal of the film was performed using a Quantum Design SQUID with a magnetic field equal to 50 Oe using warming/cooling rate of 1K/min. Measurements repeated with the same cooling rate using 100 and 150 Oe applied fields displayed a linear increase in magnetization, which was used to quantify the paramagnetic response from the NGO substrate to isolate the contribution of LPCMO. To interpret the FMR results we performed micromagnetic simulations using the Object-Oriented MicroMagnetic Framework code (OOMMF) [18]. See the supplemental material for details about the simulations.

Fig.1(a) shows the intensity map of the FMR spectrum (FMR intensity vs. field at different temperatures) while cooling the LPCMO/NGO system with the dc magnetic field applied perpendicular to the plane of the film. Four regions exhibiting different FMR features are identified. Square symbols are the resonance fields obtained from Lorentzian fits of the FMR signal. In region A (Fig. 1(b)) there is a weak signal we identified as from the electron paramagnetic resonance (EPR)—due to the Mn^{+4}-Mn^{+3} spins with a resonant field near to 3550 Oe—indicated with a diamond symbol in the Fig. 1(b). Additional two more intensity can be seen: an unexpected signal near to 3 kOe and a ferromagnetic resonance whose intensity increases at lower temperatures, both indicated with circle and square symbols, respectively, in Fig. 1(b). In region B—for temperatures below 130 K—of fig. 1(a) the FMR signal intensifies, which may be associated with increased ferromagnetic interactions. Therefore, the transition between regions A and B probably corresponds to a paramagnetic-ferromagnetic transition; corresponding temperature nearly coincides with the Curie temperature—approximately 134 K—reported in the Ref. [19] for a LPCMO thin film fabricated identically and measured by polarized neutron reflectivity. In region B, the resonance field increases with decreasing temperature to 82 K. The FMR intensity for the single resonance mode in region B is shown in Fig. 1(c).

In region C of Fig. 1(a), a second resonant mode appears. Fig. 1(d) shows an example of the FMR signal at 77 K in region C. Below 72 K the intensity of the signal decreases abruptly. This is the feature of region D in the surface map of fig. 1(a), where the signal is very weak (Fig. 1(e)). The attenuation of the signal is consistent with decoherence of the uniform resonance mode due to magnetic inhomogeneity of the strain-glass state, i.e. a distribution of strain frozen into the sample [20]. Instead of a coherent uniform mode over

long length scales, the FMR in region D arises from the mixing of a large number of local signals with different resonant fields thus broadening the linewidth and weakening the FMR intensity [21].

Fig. 1(f) shows the resistance as a function of the temperature for cooling. The sample is insulating in the temperature range that coincides with regions A and B of Fig. 1(a). Therefore, the FMR signal may result from the growth of isolated metallic ferromagnetic regions that do not exceed the percolation limit in an insulating matrix. At ~90 K the sample undergoes an insulator-to-metal transition (T_{IM}), which is coincident with an increase of the magnetization (supplemental Fig. S1) and a reduction of the coercive field due to the single to multidomain transition at T_{IM} for the LPCMO/NGO system [17,22]. Additionally, the percolation of transport evidenced by the transition to metallicity coincides with the increasing FMM component of the sample [10] as manifested in the FMR signal in region C with the appearance of a second resonance. The anomalous FMR signal (region C), its appearance and sudden increase of FMR linewidth (Fig. 2) and multiple resonance modes, may be a sign of the fluid-like behavior of the AFM-COI and FMM phases characteristic of the FPS state. The increased linewidth indicates a change of magnon relaxation rate [23] and dissipative processes or fluctuations of the ferromagnetism [2].

Fig. 2 shows the fitted data for the resonant field, linewidth, and intensity in function of temperature of the FMR signal—while cooling—obtained from the density plot of the Fig. 1(a); the Fig. 2(a) shows the change of the increasing rate of the resonant field in the transition from region A to B—nearly 130 K—indicating a possible growth of ferromagnetic regions in a paramagnetic background. The blue highlighted narrow temperature region is delimiting the region C which is shown in detail in the Fig. 2(b) where the bifurcation into two FMR

signals is evident. Both modes coexist between 82 K and 77 K. At 77 K the mode represented with dark green symbols (mode M2) tends to disappear while the resonant field of the mode represented with light green symbols (mode M1) tends to decrease at 75 K. The Fig. 2(c) shows the linewidth of the FMR signal which decreases with temperature, but suddenly increases in the same temperature window where the signal bifurcates.

The Fig. 2(d) shows the linewidth in the highlighted region. The M2 linewidth increases more abruptly, which is coherent with its premature disappearing at 77 K. This linewidth broadening could indicate a strong damped dynamics probably because of a rapid change of the ferromagnetic fraction of the sample. The M1 linewidth after a first increment between 82 K and 80 K, reach a minimum nearly to 75 K—the same temperature where its respective resonant field has a maximum—but increases newly and the FMR mode finally disappear at 72 K. This minimum could be due to the increasing of ferromagnetic region size between 80 K and 75 K. Afterwards, increases newly below 75 K due to a stronger broadening effect. The Fig. 2(e) shows the FMR intensity which increases more rapidly from 130 K, i.e., from the starting temperature of region B. However, in region C the intensity of the signal decreases abruptly while this bifurcates. This is shown in the Fig. 2(f) where the M2 mode attenuates until disappear at 77 K, which is coincident with the respective increase of the linewidth of the mode. The M1 intensity increases momentarily reaching a maximum at 75 K but decreases newly until 72 K where this mode as well disappears (for fitted data while warming see supplemental Fig. S2).

Beside the attenuation of the resonance intensities below 72 K (region D, fig. 1(a)), the magnetization saturates (for cooling) (Supplemental Fig. S1). This behavior suggests thermal excitations are insufficient to alter the magnetism (i.e., the temperature is less than

the blocking temperature) and the dynamics of the FMM phase ceases [11,24] as manifested by saturation of the magnetization, linewidth broadening, and disappearance of the FMR signal, as is shown in the Fig. 2, which occurs for the dc magnetic field applied at different angles (Supplemental Fig. S3). The decrease of the FMR intensity and linewidth broadening is consistent with the SPS associated with a metastable glass-like state of a strain-glass phase. This implies a magnetic inhomogeneity [11,13] that produces decoherence of the uniform resonance mode.

Fig. 3 shows the temperature dependence of the FMR signal and calculations of the FMR signal obtained from a micromagnetic simulation. Fig. 3(a) shows the experimental FMR signal in region A corresponding to temperatures >125 K. As commented before, besides the paramagnetic resonance of Mn^{+4}-Mn^{+3} spins (indicated with a diamond symbol at Fig. 3(a)), there exists a weak FMR signal that becomes more intense as the temperature decreases (indicated with a square symbol) and a FMR signal with intensity and resonant field almost constants (indicated with a circle symbol). As the sample is paramagnetic for temperatures > 134 K [16,19], these two FMR signals are unexpected. Intensity and resonant field of the signal indicated with the circle symbol are almost constants with temperature, this could mean that such resonance comes from spins coupled ferromagnetically with the substrate or from regions in the sample with a high Curie temperature, which is possible due to nonuniformity of the chemical profile with the depth of the film [19].

Regarding to the square symbol signal, this comes presumably from randomly located ferromagnetic bonds [25], which may serve as nucleation sites ferromagnetic regions which grow as the temperature decreases. Accordingly, we calculated the FMR signal as a function of ferromagnetic region size, using the micromagnetic modeling code

OOMMF [18]. We calculate the temporal evolution of the magnetization of the simulated sample under similar conditions of an FMR experiment. The fast Fourier transform of these curves (whose derivative is the calculated FMR signal) gives resonance frequencies, ω_0, that were converted to resonance fields, H_R, using the Kittel formula $\omega_0 = \gamma\mu_0(H_R - M_{eff})$ [26], where γ is the gyromagnetic ratio and M_{eff} is the effective magnetization, which is related to the saturation magnetization and uniaxial anisotropy [27] (see supplemental material). The results are shown in Fig. 3(b), where the resonant field obtained from the calculated FMR signal increases with the size of the ferromagnetic region. The calculated signal intensity also increases but the linewidth decreases (supplemental Fig. S4), c.f., region B of the FMR spectrum (Fig. 1(c)). Above Fig. 3(b) are shown examples of the simulated systems. In all the figures of this work, the fields of experimental curves are denoted as H, while the fields of the calculated curves are denoted as H_R, which were obtained with the procedure described before.

Fig. 3(c) shows the calculation of the FMR signal assuming the growth of percolation paths (e.g., intersecting filaments) without a preferred orientation arising from the coalescence of FMM domains. The simulated system is in the figure above where isolated ferromagnetic regions, as well as percolation paths, were included. The morphology model of separated phases for the calculations was based on the reported direct observations on similar LPCMO samples, where random nucleation and anisotropic coalescence and percolation of FMM regions in an AFM-COI matrix is observed either for cooling [10,28] or increasing magnetic field [29,30]. Fig. 3(c) shows that growth of percolation could cause the appearance of additional resonance modes, like those observed in the experiment in region C (Fig. 1(a)) which is associated with the FPS state. Assuming nucleation and growth

of ferromagnetic-metallic domains, the micromagnetic simulations reproduce the behavior of the region C FMR signal (Fig. 1(a)), as shown in Fig. 4. Fig. 4(a) shows a few experimental FMR curves from 77 K to 71 K; the dashed line is a guide to the eye of H_R vs. temperature for each mode. Fig. 4(b) shows that the temperature dependence of H_R obtained from the simulations is closely related to percolation as shown in Fig. 4(c). Since the resonant fields calculated from the percolation model are similar to the experimental data (Fig. 4(a)), we conclude that nucleation and growth of metallic inclusions give rise to multiple resonant modes in the FMR signal. This is consistent with liquid-like models previously proposed [10].

At lower temperatures (region D) the FMR signal is very weak. The decrease of the signal arises in the calculation from a concomitant increase of the Gilbert damping factor α. This produces the increase of the linewidth due to decoherence of the uniform resonance mode arising from the magnetic inhomogeneity in the presumable metastable glassy-like state due to the strain-glass transition [4,21].

Three different calculated FMR signals for different α are shown in Fig 3(e) for a system having large percolation paths, as expected at low temperatures [10]. As α increases the FMR signal is strongly attenuated as observed in region D. Thus, strong attenuation and linewidth broadening of the FMR signal (for the cooling branch) suggest strong damping of spin waves within the sample. Such damping may be due to strong spin-lattice coupling in addition to a strain-glass state that causes magnetic inhomogeneities due to the complex profile of the energy landscape in this metastable glassy state which produces decoherence of the uniform ferromagnetic resonance mode. While warming from base temperature (region D), the FMR signal remains very weak, but as the temperature increases beyond the blocking

temperature (~72 K), the signal becomes stronger and has three resonances in region C (Supplemental Fig. S2). We simulated a system with ferromagnetic percolation paths with a preferred orientation—this model was chosen, according to the direct observations for the reappearance of the AFM-COI phase in FMM matrix reported previously for LPCMO, where elongated and oriented antiferromagnetic paths grow in a presumably martensitic transformation [29,30]. The results are shown in Fig. 3(d) (the morphologies of the magnetic phase are shown on the bottom of the figure) where three well-differentiated resonant modes, arising from FMM paths of different sizes, can be identified corresponding to the data (for region C, warming).

Since the FMR signal for region C, while warming is different from cooling, our results suggest that phase morphology evolves differently for each of these branches. This difference in paths could be the result of the phase transition in an energy landscape with multiple equilibrium states created by the competition between phases [11,31]. In the cooling branch, the FMM domains nucleate and grow in an AFM-COI matrix without a preferred orientation or order. The nucleation process is driven mainly by quenched disorder induced by Pr chemical doping [29]. However, in the warming branch, the AFM-COI regions nucleate in an FMM matrix causing the appearance of an anisotropic epitaxial strain. This causes a preferred orientation growth of the AFM-COI region [29]. The most energetically favorable recovery of the AFM-COI phase could be a martensitic transformation [29,32], which can only be achieved at higher temperatures than that of the strain-glass state (region D). Hence, in region C for the warming branch, the AFM-COI orientated regions grow with temperature, yielding elongated FMM regions of different widths, therefore producing a distinguishable FMM domain morphology and thus a different FMR response (supplemental

Fig. S5), probably by the demagnetization effect, since our calculations suggest that without demagnetizing energy the FMR signal in region C does not have multiple modes. (supplemental Fig. S6).

This is confirmed by the dependence on demagnetizing factors of more general formulas for the ferromagnetic resonance frequency [27,33]. Demagnetization could lead to the FMR signal being highly susceptible to the morphology of FMM domains—i.e., it is different for elongated (while warming) or randomly coalesced (while cooling) domains, in the case of region C. In regions B and A the signal is the same for the cooling and warming branches due to similar morphology evolution. This also suggests that the demagnetization energy could have a leading role in the energy landscape profile, also affecting the phases competition. .

In summary, we report a rich FMR spectrum from a single crystalline LPCMO film, a prototypical phase-separated manganite. The FMR spectrum exhibits zero to multiple resonances with varying intensity and linewidth at different temperatures. Using micromagnetic simulation, we developed a model for the FMM and AFM-COI phase separated material which includes a temperature-dependent change of phase fraction, morphology, and percolation. The FMR spectra calculated from the simulation qualitatively reproduce the observed richness of the measured FMR spectra. The simulations also reveal that the multiple resonances only appear when we include the demagnetization energy in the calculations. Such energy could be important in the energy landscape responsible for phase separation. In addition, probably because of demagnetization, the FMR signal is highly susceptible to the morphology of the phase separation. We conclude that as the film is cooled from high temperature, patches of FMM materials nucleate (randomly), grow, and percolate

forming stripes eventually coalescing into a full FMM state. The spin dynamics change continuously as the FMM domains grow. Upon percolation (as observed in the transport data), the spin dynamics change dramatically—the FMR linewidths become very broad indicating strongly damped dynamics. However, in warming, the recovery of the AFM-COI phase may occur following an ordered martensitic transformation, instead of randomly as in cooling, yielding orientated FMM percolation paths. Our FMR results show that morphology evolves differently for cooling or warming in the fluid-phase-separated state.

Acknowledgments

This is highly collaborative research. The experiments were conceived jointly, the data was extensively debated, and the paper was written by multiple iterations between all the coauthors. This research used resources at the Spallation Neutron Source, a DOE Office of Science User Facility operated by the Oak Ridge National Laboratory. J.G.R. and D.C-C. acknowledge support from Facultad de Ciencias and Vicerrectoría de Investigaciones Universidad de los Andes. Convocatoria Facultad de Ciencias, proyecto código INV-2020-104-2080. E.S. was supported by the U.S. Department of Energy (DOE), Basic Energy Sciences, Materials Sciences, and Engineering Division. A.B. acknowledge support by NSF DMR-1410237. M.R.F. was supported by the US DOE, Basic Energy Sciences, Division of Scientific User Facilities. The research at UCSD was supported by the Office of Basic Energy Science, U.S. Department of Energy, BES-DMS funded by the Department of Energy's Office of Basic Energy Science, DMR under grant DE FG02 87ER-45332.

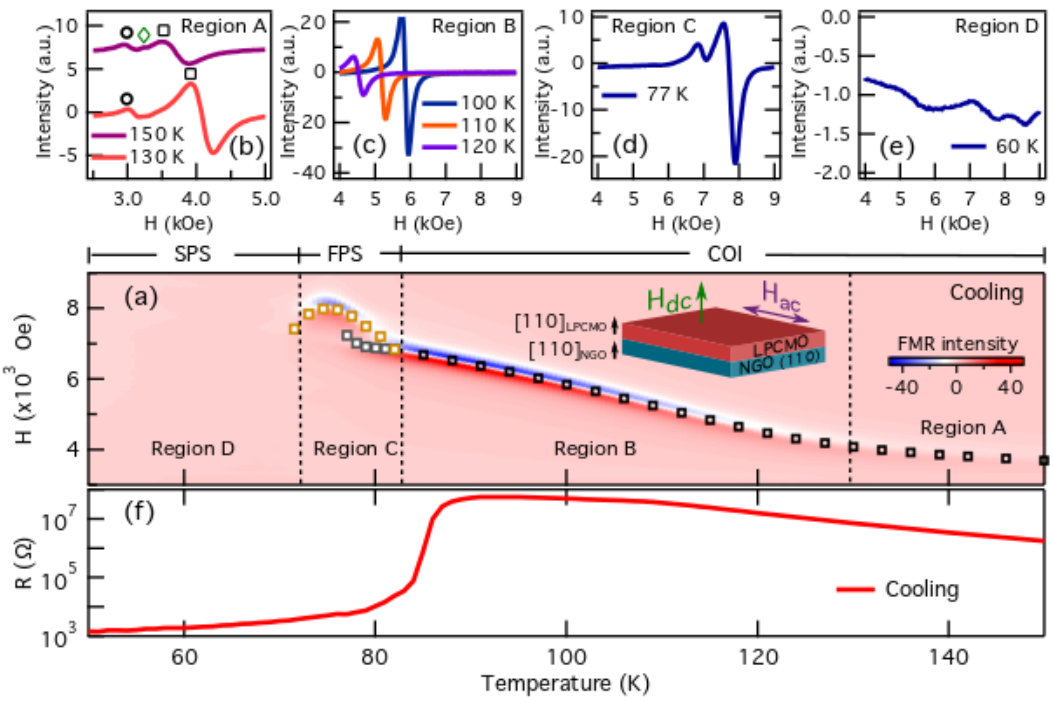

Figure 1. (a) Density plot of the FMR signal as a function of temperature for the cooling. In the temperature regions A, B, C, and D qualitatively different behavior is observed. Square symbols correspond to fitted resonant field at selected temperatures. The various resonance fields are obtained from the fitted FMR signals (Fig. 2). The inset shows the orientation of the LPCMO thin film and NGO substrate, as well as the orientation of the dc magnetic field (H_{dc}) and microwave field (H_{ac}) in the FMR experiment. (b), (c), (d), and (e) show FMR curves for specific temperatures in regions A, B, C, and D, respectively. The EPR and FMR signals in the figure (b) are denoted with diamond and square symbols, respectively. The circle symbol indicates an unexpected FMR signal. (f) Resistance as a function of temperature for cooling.

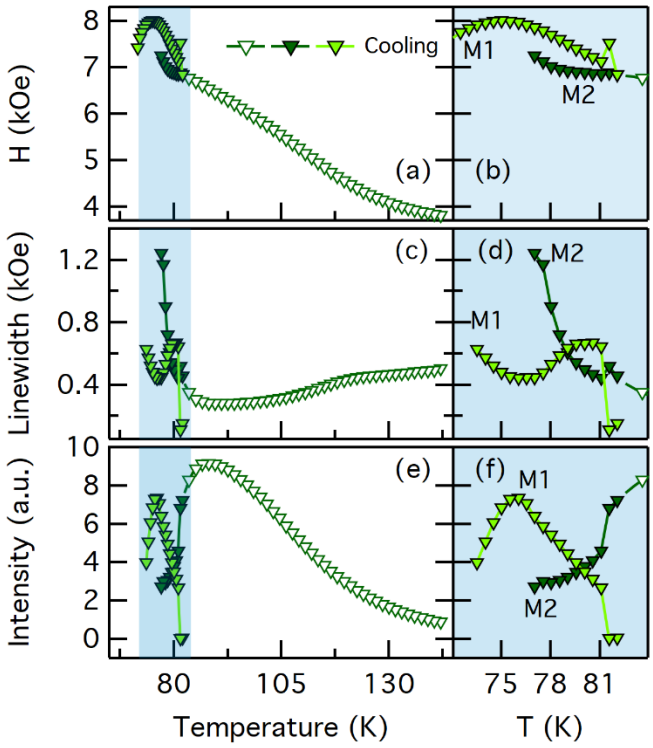

Figure 2. (a) Resonant field, (c) linewidth and (e) intensity data fitted from the FMR density plot of the Fig. 1(a). Respective highlighted narrow temperature regions are shown in detail in the figures (b), (d) and (f). Both modes in such region are denoted as M1 and M2.

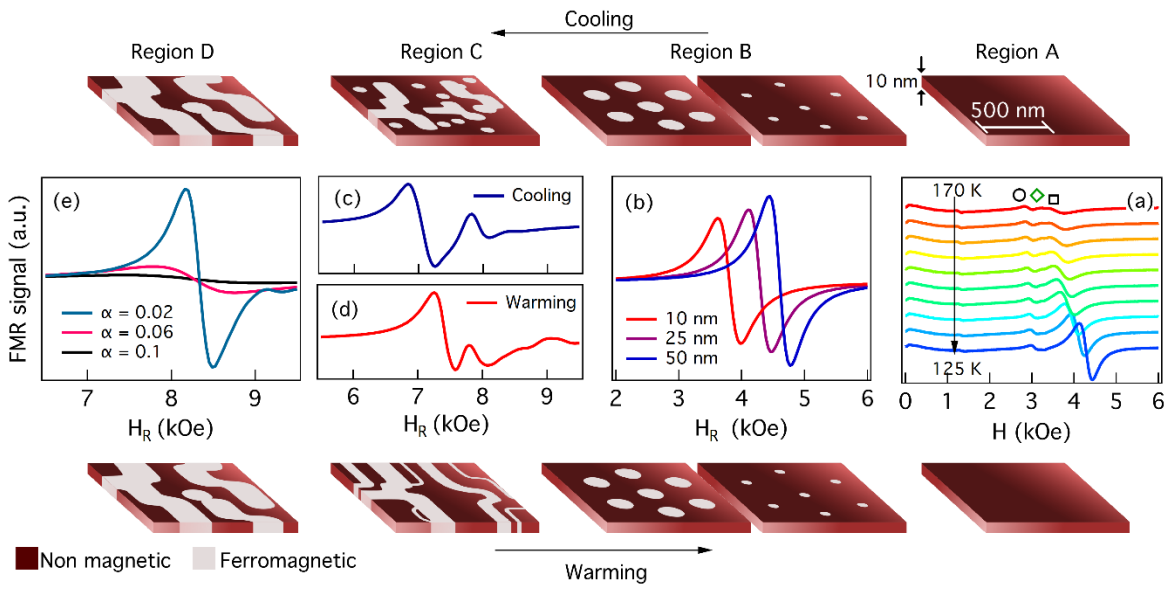

Figure 3. (a) Experimental FMR signal in the paramagnetic region A. Symbol diamond indicates the typical EPR signal. Circle and square symbols indicate weak FMR signals. (b) Calculated FMR signal (denoted by H_R) in region B, where the size of ferromagnetic regions increases while cooling and decreases while warming. (c) FMR simulation in region C for cooling, assuming the percolation of ferromagnetic regions (the upper figure shows the simulated system). (d) FMR simulation in region C for warming (the lower figure shows the simulated system). (e) FMR simulation for a system where ferromagnetic regions percolate. The FMR signal becomes weaker (like in the experimental region D) with increasing Gilbert damping.

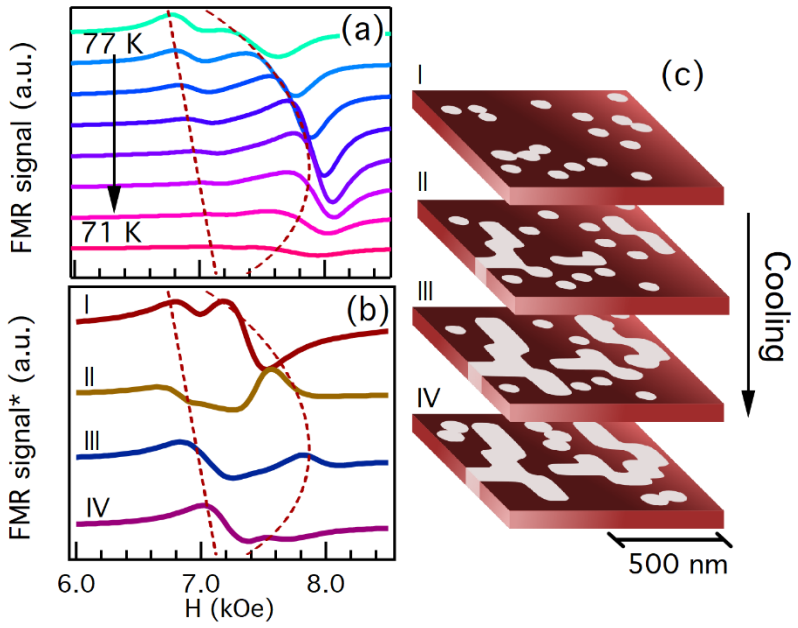

Figure 4. (a) Experimental FMR signal between 77 K and 71 K (region C) for cooling. (b) FMR simulation for the modeled four systems of (c).

[1] M. Uehara, S. Mori, C. H. Chen, and S.-W. Cheong, Nature **399**, 560 (1999).

[2] L. Ghivelder and F. Parisi, Phys. Rev. B **71**, 184425 (2005).

[3] S. Singh, G. Sharma, M. K. Thakur, P. K. Siwach, P. Kumar Tyagi, K. K. Maurya, and H. K. Singh, AIP Adv. **5**, 027131 (2015).

[4] P. A. Sharma, S. B. Kim, T. Y. Koo, S. Guha, and S. W. Cheong, Phys. Rev. B **71**, 224416 (2005).

[5] T. Dhakal, J. Tosado, and A. Biswas, Phys. Rev. B **75**, 092404 (2007).

[6] A. Shakya and A. Biswas, J. Appl. Phys. **127**, 213902 (2020).

[7] H. Zhou, L. Wang, Y. Hou, Z. Huang, Q. Lu, and W. Wu, Nat. Commun. **6**, 8980 (2015).

[8] T. Z. Ward, J. D. Budai, Z. Gai, J. Z. Tischler, L. Yin, and J. Shen, Nat. Phys. **5**, 885 (2009).

[9] E. Dagotto, T. Hotta, and A. Moreo, Phys. Rep. **344**, 1 (2001).

[10] L. Zhang, C. Israel, A. Biswas, R. . Greene, and A. de Lozanne, Science (80-.). **298**, 805 (2002).

[11] W. Wu, C. Israel, N. Hur, S. Park, S.-W. Cheong, and A. de Lozanne, Nat. Mater. **5**, 881 (2006).

[12] Y. Tomioka and Y. Tokura, Phys. Rev. B **70**, 014432 (2004).

[13] K. F. Wang, Y. Wang, L. F. Wang, S. Dong, D. Li, Z. D. Zhang, H. Yu, Q. C. Li, and J.-M. Liu, Phys. Rev. B **73**, 134411 (2006).

[14] V. G. Sathe, A. Ahlawat, R. Rawat, and P. Chaddah, J. Phys. Condens. Matter **22**, 176002 (2010).

[15] B. Rana and Y. Otani, Commun. Phys. **2**, 90 (2019).

[16] S. Singh, M. R. Fitzsimmons, T. Lookman, J. D. Thompson, H. Jeen, A. Biswas, M. A. Roldan, and M. Varela, Phys. Rev. Lett. **108**, 077207 (2012).

[17] H. Jeen and A. Biswas, Phys. Rev. B **83**, 064408 (2011).

[18] M. J. Donahue and D. . Porter, *OOMMF User's Guide, Version 1.0. Interagency Report NISTIR 6376, National Institute of Standards and Technology, Gaithersburg, MD (Sept 1999)* (n.d.).

[19] S. Singh, M. R. Fitzsimmons, T. Lookman, H. Jeen, and A. Biswas, Phys. Rev. B **90**, 060407 (2014).

[20] X. Ren, Phys. Status Solidi B **251**, 1982 (2014).

[21] A. Barman and J. Sinha, *Spin Dynamics and Damping in Ferromagnetic Thin Films and Nanostructures* (Springer International Publishing, Cham, 2018).

[22] S. Singh, J. W. Freeland, M. R. Fitzsimmons, H. Jeen, and A. Biswas, Sci. Rep. **6**, 29632 (2016).

[23] X. Liu and J. K. Furdyna, J. Phys. Condens. Matter **18**, R245 (2006).

[24] B. D. Cullity and C. D. Graham, in *Introd. to Magn. Mater.* (John Wiley & Sons, Inc., Hoboken, NJ, USA, 2009), pp. 359–408.

[25] J. Deisenhofer, D. Braak, H.-A. Krug von Nidda, J. Hemberger, R. M. Eremina, V.

A. Ivanshin, A. M. Balbashov, G. Jug, A. Loidl, T. Kimura, and Y. Tokura, Phys. Rev. Lett. **95**, 257202 (2005).

[26] J. M. D. Coey, *Magnetism and Magnetic Materials* (Cambridge University Press, Cambridge, 2010).

[27] M. J. Hurben and C. E. Patton, J. Appl. Phys. **83**, 4344 (1998).

[28] Y. Zhu, K. Du, J. Niu, L. Lin, W. Wei, H. Liu, H. Lin, K. Zhang, T. Yang, Y. Kou, J. Shao, X. Gao, X. Xu, X. Wu, S. Dong, L. Yin, and J. Shen, Nat. Commun. **7**, 11260 (2016).

[29] F. Jin, Q. Feng, Z. Guo, D. Lan, L. Wang, G. Gao, H. Xu, B. Chen, F. Chen, Q. Lu, and W. Wu, Phys. Rev. Mater. **1**, 064406 (2017).

[30] Q. Feng, F. Jin, H. Zhou, L. Wang, W. Meng, K. Zhang, J. Wang, J. Zhang, Y. Hou, Q. Lu, and W. Wu, Adv. Mater. **30**, 1805353 (2018).

[31] S. Singh, P. Kumar, P. K. Siwach, P. K. Tyagi, and H. K. Singh, Appl. Phys. Lett. **104**, 212403 (2014).

[32] V. Podzorov, B. G. Kim, V. Kiryukhin, M. E. Gershenson, and S.-W. Cheong, Phys. Rev. B **64**, 140406 (2001).

[33] C. Kittel, Phys. Rev. **73**, 155 (1948).